Comparative Analysis of CFD Modeling and Process Simulation for Pyro-Gasification of Biomass

Diakaridia Sangaré [a,b,c,*] Verónica Belandria,[c,d] Stéphane Bostyn,[c,d] and Mario Moscosa-Santillan [b,*]

** Corresponding authors: diakaridia.sangare@cirad.fr, mario.moscosa@uaslp.mx*

DOI: 10.15376/biores.20.2.2844-2870

GRAPHICAL ABSTRACT

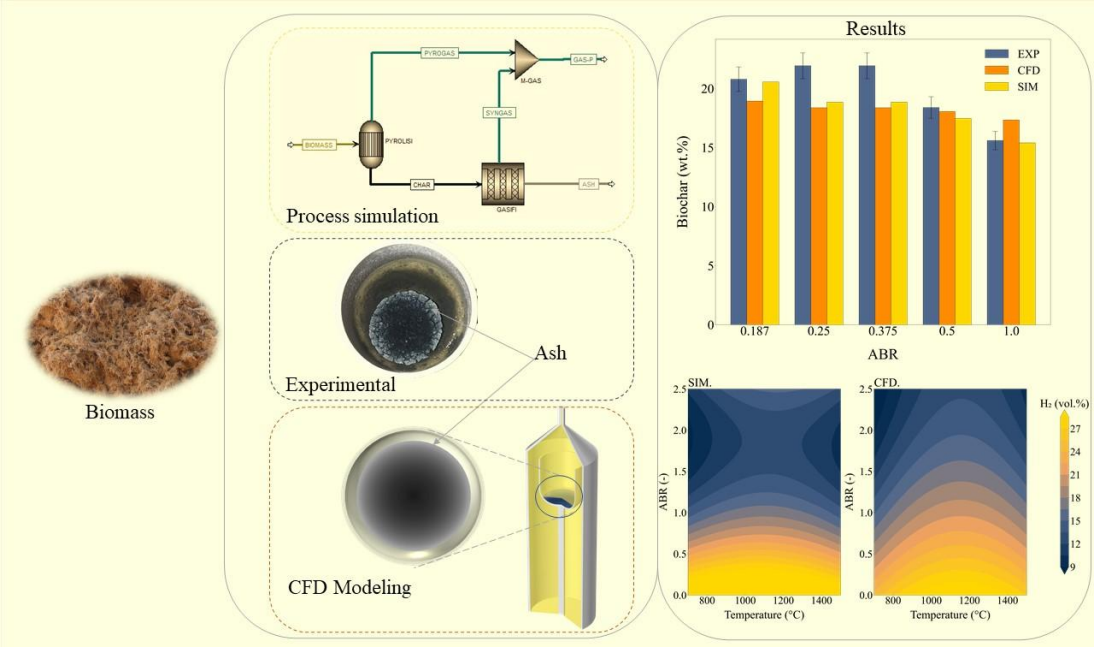

Comparative Analysis of CFD Modeling and Process Simulation for Pyro-Gasification of Biomass

Diakaridia Sangaré [a,b,c,*] Verónica Belandria,[c,d] Stéphane Bostyn,[c,d] and Mario Moscosa-Santillan [b,*]

A comparative analysis of Computational Fluid Dynamics (CFD) modeling and process simulation (SIM) was carried out to evaluate biomass pyro-gasification, using experimental data from agave bagasse (AB) as a case study. Experimental data were obtained *via* thermogravimetric analysis (TGA) under varying conditions, including non-isothermal (700 to 1000 °C) and isothermal (900 °C and 950 °C) gasification at different air-to-biomass ratios (ABR). CFD modeling in COMSOL Multiphysics focused on micro-scale mass and heat transfer phenomena, while Aspen Plus simulations provided macro-scale process insights. Results showed that SIM closely matched experimental product yields under isothermal conditions (maximum deviation: 4.23 wt.%), while CFD excelled in predicting gas composition under non-isothermal conditions (*e.g.*, H_2 deviation: 3.29 vol.%). Sensitivity analysis showed how temperature and ABR are critical factors that influence the product yield and gas composition, highlighting the strengths of each modeling approach. These findings underline the potential of integrating CFD and SIM approaches for improving the accuracy of biomass conversion modeling, paving the way for optimized process designs and scalable industrial applications.

DOI: 10.15376/biores.20.2.2844-2870

Keywords: Biomass; Pyrolysis; Gasification; CFD Modeling; Process simulation; Sensitivity analysis

*Contact information: a: CIRAD, UPR BioWooEB, 73 rue Jean-François Breton, F-34398 Montpellier, France; b: Facultad de Ciencias Químicas Universidad Autónoma de San Luis Potosí Av. Dr. Nava # 6, Zona Universitaria San Luis Potosí, S.L.P., CP: 78210, México; c: Institut de Combustion, Aérothermique, Réactivité, et Environnement (ICARE)-CNRS UPR3021, 1C avenue de la recherche scientifique 45071 Orléans Cedex 2, France; d: Université d'Orléans, Institut Universitaire de Technologie, 16 rue d'Issoudun BP16724 45067 Orléans Cedex 2, France; * Corresponding authors: diakaridia.sangare@cirad.fr, mario.moscosa@uaslp.mx*

INTRODUCTION

The rising global energy demand and environmental concerns associated with fossil fuel use have intensified the search for sustainable energy alternatives (Shahbaz *et al.* 2017; Okoro *et al.* 2020; Ajorloo *et al.* 2022). Biomass, as a renewable energy source, offers a significant advantage due to its potential to reduce net CO_2 emissions and its abundance across diverse regions (Ajorloo *et al.* 2022). However, using biomass as an energy source requires efficient conversion processes. In this field, thermochemical methods, such as pyrolysis, gasification, and combustion, are the most widely used technologies (Nsaful *et al.* 2013; Liu *et al.* 2017). Among thermochemical conversion processes, pyrolysis and gasification are efficient methods to convert biomass into valuable products such as synthesis gas, biochar, and bio-oil. Gasification is particularly

versatile, enabling the production of synthesis gas (syngas) as a precursor for energy generation and chemical synthesis (Nsaful *et al.* 2013; Liu *et al.* 2017). The syngas can be used as a source of energy (electricity, hydrogen) and in the manufacture of high-value-added products in the chemical industry (Basu 2018; Sangaré *et al.* 2022).

Pyrolysis is the initial stage of gasification, and it plays a critical role in determining product distribution, including non-condensable gases (NCG), solid carbon (biochar), and condensable vapor (bio-oil). Factors such as temperature, heating rate, and the air-to-biomass ratio (ABR) strongly influence the yield of the products. In addition, bio-oils, including tars, reach their maximum yield between 400 and 700 °C, before undergoing thermal cracking into lighter gases at temperatures above 700 °C (Lin *et al.* 2016; Sangaré *et al.* 2022). Although the increased temperature and heating rates generally favor gas production, they also complicate process optimization by favoring tar formation, a major operational challenge due to its tendency to condense and obstruct pipelines (Devi *et al.* 2005). In addition, these complex mixtures, which include polycyclic aromatic hydrocarbons (PAHs), require advanced mitigation techniques, including thermal and catalytic cracking (Li and Suzuki 2009; Yan *et al.* 2014; Zeng *et al.* 2020).

To solve these challenges, the pyro-gasification process offers a promising solution. This process consists of two main stages: an initial pyrolysis stage, where biomass is thermally decomposed to produce biochar, non-condensable gases, and condensable vapor (including tar), followed by partial oxidation of condensable vapor and char. During the partial oxidation stage, the biochar and tars generated during pyrolysis are converted into syngas through thermal oxidation processes (Okoro *et al.* 2020; Sangaré *et al.* 2024a).

Although gasification and pyro-gasification are similar processes, the distribution of products can vary depending on the operating conditions. In both cases, product distribution is strongly influenced by heating rate, gasifying agent, and temperature. Numerous studies have been conducted on the gasification of charcoal using various gasifying agents, including air (Wang *et al.* 2008; Zhang *et al.* 2015; Zhang *et al.* 2017), steam (Moghadam *et al.* 2014; Jayaraman and Gökalp 2015; Elorf *et al.* 2019), oxygen (Niu *et al.* 2014), carbon dioxide (Gao *et al.* 2016b), supercritical water (Guo *et al.* 2015), and so forth. Generally, gasification with oxygen, steam, carbon dioxide, or supercritical water yields syngas with higher heating values (HHV) than air gasification. However, air gasification remains the most studied and applied method due to the low cost of air, the reaction process's simplicity, and the reactor's straightforward design (Gao *et al.* 2016a; Okoro *et al.* 2017).

Despite the potential of pyro-gasification, product optimization and tar formation challenges remain significant, as these depend heavily on operating parameters. While experimental studies provide valuable data, their interpretation is often complicated by the difficulty of extrapolating laboratory-scale results to industrial applications. In this context, modeling and simulation have become essential tools. Various modeling approaches have been used to study biomass thermochemical conversion, including thermodynamic equilibrium, kinetic, and Computational Fluid Dynamics (CFD) models.

Thermodynamic equilibrium models are effective for establishing theoretical limits, offering insights into maximum efficiency and outputs under ideal conditions. However, their reliance on simplifying assumptions restricts their applicability to non-equilibrium scenarios, such as low-temperature oxidation or systems with complex reaction kinetics (Beheshti *et al.* 2015; Patra and Sheth 2015; Gmehling *et al.* 2019;

Safarian *et al.* 2019). Kinetic models, on the other hand, provide detailed insights into reaction mechanisms and rates by incorporating dynamic chemical interactions (Upreti 2017; Gmehling *et al.* 2019; Ascher *et al.* 2022). However, these models often fall short in addressing spatial and temporal variations within reactors.

Modeling and simulation approaches have thus become indispensable for navigating these complexities and bridging the gap between laboratory findings and industrial-scale applications. CFD excels in resolving spatially and temporally detailed heat and mass transfer phenomena, while process simulation (SIM) offers a macroscopic perspective, integrating equilibrium and kinetic assumptions (Vyazovkin *et al.* 2014; Van Hoecke *et al.* 2023; Sangaré *et al.* 2024b). Despite extensive research on these individual approaches, comparative studies evaluating their predictive accuracies under varying gasification conditions remain scarce.

This study aims to bridge this gap by conducting a comparative analysis of CFD modeling using COMSOL Multiphysics and SIM using Aspen Plus for the pyro-gasification of agave bagasse, a by-product of mezcal production. The objective is also to highlight their respective strengths and limitations in predicting pyro-gasification behavior. Experimental data obtained through thermogravimetric analysis (TGA) under isothermal and non-isothermal conditions were used to validate and evaluate model performance. The specific objectives were (1) to assess the accuracy of CFD and SIM in predicting product yields (biochar, bio-oil, and non-condensable gases) and gas compositions; (2) to identify the operational conditions where each method performs optimally; (3) to provide insights into integrating CFD and SIM for improved modeling frameworks. By addressing these objectives, the study contributes to the development of more accurate and scalable modeling strategies for biomass pyro-gasification, facilitating process optimization and reducing the environmental footprint of bioenergy production.

EXPERIMENTAL

Feedstock Properties and Description

This study focused on agave bagasse (AB), a by-product of mezcal production. The AB was collected from the "Santa Teresa" distillery in San Luis Potosí, Mexico. It was initially air-dried at ambient temperature (28 to 35 °C) for approximately one week to reduce moisture content, followed by drying at 105 °C for 24 h to achieve a constant mass. The dried material was then milled to a particle size between 0.1 and 1 mm, ensuring uniformity for thermochemical conversion experiments. A char was produced from AB through pyrolysis at 700 °C, using a heating rate of 20 °C/min under argon atmosphere until the final temperature was reached. The properties of this char, along with the physicochemical characteristics of raw AB, are presented in Table 1, and a detailed description of this feedstock is available in previous publications (Sangaré *et al.* 2024a,b).

Experimental Setup and Analytical Methods

The experiments were conducted using a Netzsch STA 449 F3 Jupiter thermal analyzer, coupled with an SRA SOLIA 490 μ-GC, equipped with three thermal conductivity detectors (TCD) to allow comprehensive gas quantitation and analysis. The experimental setup and analytical methodology used were described in a previous study (Sangaré *et al.* 2024a). For each experiment, around 150 ± 2 mg of biomass; was placed in a crucible. The biomass samples were heated from room temperature to 700 °C at 40 °C/min, with argon as the carrier gas at a flow rate of 20 mL/min. For char oxidation experiments, air was introduced at 3 mL/min from 700 to 1000 °C under non-isothermal conditions to evaluate all four biomass types. Additionally, separate isothermal gasification experiments were conducted at 900 and 950 °C with an airflow rate of 4 mL/min, focusing exclusively on AB to investigate its behavior under these specific conditions.

CFD Modeling Strategy

Reactor geometry

In this CFD simulation, the reactor geometry is shown in Fig. 1. The reactor consists of an alumina (Al_2O_3) crucible integrated into a thermogravimetric analyzer, with a total volume of 5 mL. The geometric models were created using COMSOL Multiphysics®6.2. Based on the reactor geometry characteristics and to reduce computational time, a 2D axisymmetric model was employed, adjusted to correspond to the dimensions of the reactors used experimentally to simulate the entire pyro-gasification process. The mesh independence study was conducted in the previous publication (Sangaré *et al.* 2024b), and the final refined mesh used in this work is presented in Fig. 1.

Table 1. Physicochemical Properties and Compositions of AB

		AB	Char 700 °C	Char 800 °C	Char 900 °C	Char 1000 °C
Proximate Analysis (wt%)						
Moisture content (MC)		4.81±1.21	-	-	-	-
Volatile matter (VM)		77.91±1.42	23.30 ± 1.58	-	-	-
Fixed carbon (FC) [a]		18.76±1.61	65.30 ± 2.18	85.61 ± 3.50	87.92 ± 3.20	86.60 ± 1.38
Ash		3.34± 0.43	12.90 ± 0.84	14.39 ± 2.19	12.08 ± 3.20	13.40 ± 1.38
Ultimate Analysis (wt%)						
Carbon		45.14 ± 0.21	76.75 ± 0.06	77.40 ± 1.58	80.31 ± 2.32	79.40 ± 1.88
Hydrogen		5.50 ± 0.23	1.90 ± 0.00	1.41 ± 0.01	0.94 ± 0.00	0.75 ± 0.01
Nitrogen		0.31± 0.10	0.61 ± 0.06	0.86 ± 0.07	0.88 ± 0.04	0.98 ± 0.04
Sulfur		nd.	nd.			
Oxygen [a]		45.71± 0.22	7.84 ± 0.12	7.20 ± 1.52	7.78 ± 2.28	5.10 ± 1.90
Chemical Analysis (wt%) *						
Extractives [d] (wt.)	TGL	1.10				
	TANN	0.40				
Lignin [d] (wt.%)	LIGC	5.01				
	LIGH	8.12				
	LIGO	1.12				
Hemicellulose (wt.%)		43.81				
Cellulose [a] (wt.%)		40.74				
HHV(MJ/kg)		**16.5±0.3**				
Bulk density[b] (kg/m^3)		673.4	358			
Actual density[c] (kg/m^3)		1559	-			
Porosity (-)		0.57	0.74			
Average particle size (mm)		0.5	0.1			
Thermal conductivity (W/m-K)			$k_b = 0.035 + 1.73 \times 10^{-4}T$			
			k_{char} =0.08-3×10^{-4}T			
Heat capacity (J/kg·K)			$C_{pchar} = 1003.2 + 2.09\,T$			
			$C_{pb} = 103.1 + 3.87T$			
Standard analysis methods						
Moisture content (MC)			EN 14774-3: 2009: E			
Volatile matter (VM)			EN 15148: 2009 E			
Ash content			EN 14775: 2009: E			
Fixed carbon (FC)			FC = 100 − [MC + VM+ Ash]			
Proximate analysis			CEN/TS 15104:2005			
Higher heating values (HHV)			ASTM D5865-12			
Bulk density			ASTM E873-82			

nd: not detected (<0.1%); [a]:by difference; [b]:bulk density was estimated considering that the porosity is the space between the biomass particles; [c]:actual density estimated from biomass chemical composition, [d]: methodology described by Debiagi *et al.* (2015) and [*]: Procedures described by Li *et al.* (2004).

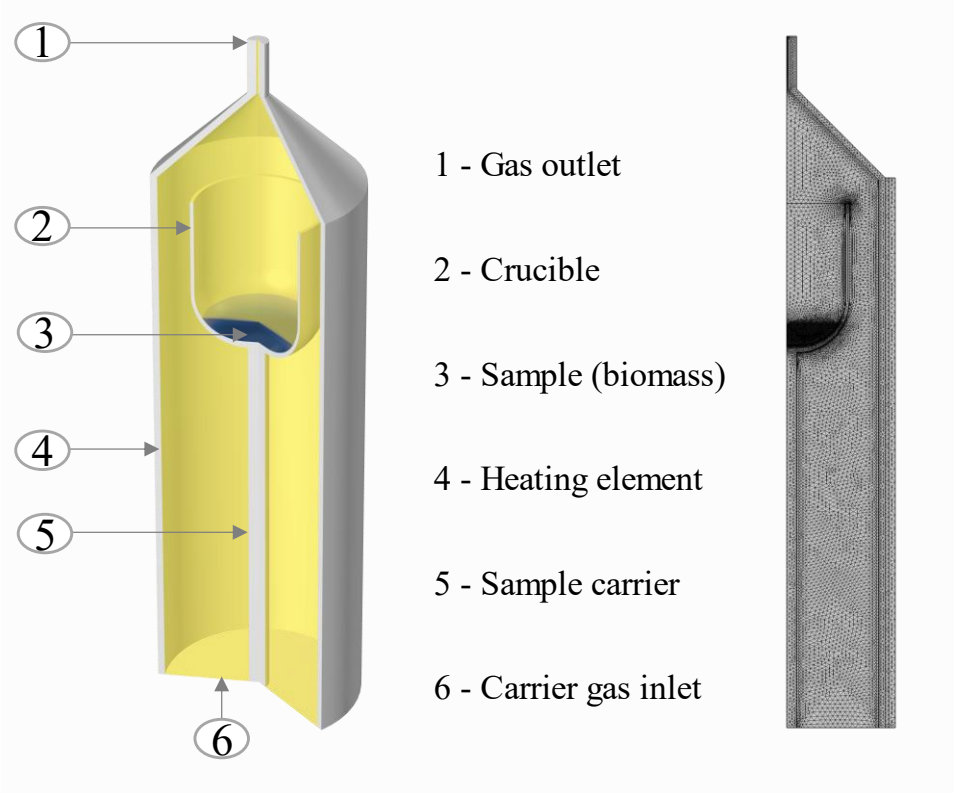

Fig. 1. The reactor geometry: a) CFD domain and b) 2D-axisymmetric meshed

CFD Numerical Model

CFD modeling was carried out using COMSOL Multiphysics® 6.2. The numerical modeling included drying, devolatilization, and secondary reactions, such as tar cracking and the subsequent char oxidation and homogeneous reactions in fluid phases. Due to its characteristics, the system was considered a porous medium system. To describe the flow in the porous medium, Darcy's law was used in combination with Brinkman's equations, which allowed the incorporation of the velocity and pressure interaction in the porous medium associated with the solid phase. Equation (1) describes fluid flow in a porous medium.

$$\frac{1}{\varepsilon_p}\rho\left(\frac{\partial u}{\partial t}+(u\cdot\nabla)\frac{u}{\varepsilon_p}\right)=-\nabla p+\nabla\cdot\left(\frac{1}{\varepsilon_p}\left(\mu(\nabla u+(\nabla u)^{\tau})-\frac{2}{3}\mu(\nabla\cdot u)I\right)\right)-\left(\frac{\mu}{\kappa}+\frac{Q_m}{{\varepsilon_p}^2}\right)u+F \quad (1)$$

where u is velocity (m/s), μ is fluid viscosity (Pa-s), ρ is fluid density (kg/m^3), ε_p is porosity (-), p is pressure (Pa), κ is permeability (m^2), and F represents external forces (kg/(m^2·s^2)). Additionally, I and τ denote the identity matrix and the transpose operator, respectively. Furthermore, Q_m is the mass source (kg/(m^3·s). Equation 1 is always solved together with the continuity Eq. 2.

$$\frac{\partial(\varepsilon_p\rho)}{\partial t}+\nabla\cdot(\varepsilon_p\rho u)=Q_m \quad (2)$$

There is no mass source term, as (Q_m=0). In porous media, the κ controls the

directional movement of flow, establishing a linear relationship between pressure drop (p) and the flow velocity field (u).

$$-\nabla p = \mu \frac{\boldsymbol{u}}{k} \tag{3}$$

Darcy flow can be characterized by Kozeny-Carman equation, which estimates the permeability of a porous medium based on the average particle diameter (d_p) and porosity (ε_p) (Bear and Braester 1972).

$$\kappa = \frac{{d_p}^2}{180} \frac{{\varepsilon_p}^3}{(1-\varepsilon_p)^2} \tag{4}$$

The Brinkman Equation (Eq. 1), combined with the continuity Eq. 2 and the species transport Eq. 5 in porous media, provides a comprehensive framework for modeling biomass reactions,

$$\frac{\partial(\phi_i c_i)}{\partial t} + \frac{\partial(\rho c_{p,i})}{\partial t} + u \cdot \nabla c_i = D_{e,i} \cdot \nabla^2 c_i + R_i \tag{5}$$

where c_i represents the concentration of species i (mol/m^3) in the fluid phase, t is time (s), $c_{P,\,i}$ denotes the quantity adsorbed into biomass bed (mol/kg of the solid), ϕ_i is volume fraction of fluid (-), ρ is the liquid's bulk density (kg/m^3), $D_{e,\,i}$ is the diffusion coefficient (m^2/s), and R_i describes the reaction rate model (mol/m^3·s). The value of R_i is given by the following equation,

$$R_i = C_i k_i e^{\frac{-E_i}{RT}} \tag{6}$$

where k_i is the pre-exponential factor (1/s), E_i is the activation energy (J/mol), R is the gas constant (J/mol-K), and T is the temperature (K).

The value of $D_{e,i}$ was obtained from literature correlations (Guizani *et al.* 2015; Mermoud *et al.* 2006), and it is expressed as follows,

$$D_{e,i} = \frac{\varepsilon_p}{\gamma} \frac{1}{\left(\frac{1}{D_{Knudsen,i}} + \frac{1}{D_{AB,i}}\right)} \tag{7}$$

$$D_{AB,i} = 1.67 \times 10^{-5} \left(\frac{T}{298}\right)^{1.75} \tag{8}$$

$$D_{Knudsen,i} = 0.97 \left(\frac{d_p}{2}\right) \sqrt{\frac{T}{M_i}} \tag{9}$$

where $D_{AB,i}$ represents the binary diffusivity (m^2/s) of the single-phase diffusion coefficient for species A (reactive gases) as it migrates through a carrier gas B (Argon). The $D_{Knudsen,i}$ represents the Knudsen diffusion coefficient, which accounts for molecular transport in porous media. This occurs when the mean free path of gas molecules is comparable to or larger than the pore diameter, leading to more frequent molecule-wall collisions than intermolecular collisions (Guizani *et al.* 2015). M_i is the molecular mass (g/mol). The tortuosity factor γ accounts for the reduced diffusivity resulting from the impediments caused by particle grains, which hinder Brownian motion. For saturated media, the effective tortuosity can be determined using the Millington and Quirk model (1961),

$$\gamma = {\varepsilon_p}^{-1/3} \tag{10}$$

$$\varepsilon_p = 1 - \frac{\rho_b}{\rho_r} \quad (11)$$

The heat transfer equation is given as follows,

$$\boldsymbol{\varepsilon_p}\rho C_{p,f}\frac{\partial T}{\partial t} + \rho C_{p,f}\boldsymbol{u}.\nabla T + \nabla \cdot \boldsymbol{\varepsilon_p} k_f \nabla T = Q \quad (12)$$

$$\phi_s \rho_s C_{p,s}\frac{\partial T}{\partial t} - \nabla \cdot \phi_s k_s \nabla T = Q \quad (13)$$

where C_{pf} and $C_{ps,}$ represent the heat capacities (J/kg-K) of fluid and solid, respectively, k_f and k_s are the thermal conductivities (W/m-K) of fluid and solid, and Q denotes an external heat source (W/m^3). This CFD modeling did not include heat generated by pressure changes due to viscous dissipation.

Chemical Kinetics Applied to CFD Modeling of Pyrolysis

The biomass pyrolysis process begins with moisture evaporation during drying, followed by devolatilization, which produces volatile products, including non-condensable and condensable gases, bio-oil, and biochar containing fixed carbon solids and ash. Secondary reactions, such as char and tar cracking, follow. The multi-step kinetic mechanism scheme described in a previous study (Sangaré *et al.* 2024b) was used to model this process.

Reaction kinetics of char oxidations

After the biomass was pyrolyzed, the resulting char was oxidized by injecting a gasifying agent. Char oxidation involves both heterogeneous and homogeneous reactions. The heterogeneous reaction of char with the surrounding gaseous species such as O_2, CO_2, and H_2O is a complex process involving specific interactions such as char-O_2, char-CO_2, and char-H_2O reactions (Nguyen *et al.* 2018; Fatehi *et al.* 2019; Yang *et al.* 2022). The kinetic details are summarized in Table 2.

In R- 1, the parameter Z is defined from Eq. 14.

$$\mathrm{z} = \frac{\mathrm{c_{CO}}}{\mathrm{c_{CO_2}}} = 2.5 \times 10^3 \mathrm{e}^{-\frac{6249}{\mathrm{T}}} \quad (14)$$

Process Simulation Strategy

In gasification modeling using Aspen Plus®, two primary approaches can be applied: one that assumes the complete equilibrium of the system and another that applies a semi-detailed kinetic mechanism (Beheshti *et al.* 2015). A semi-detailed kinetic method was employed because the system may not strictly achieve equilibrium under the simulation conditions evaluated in this study. This approach allows for estimating the product yield and gas composition during the pyrolysis stage, followed by the different kinetics of oxidation reactions.

Thermodynamic model and physical properties

Process simulations were conducted using Aspen Plus® and the Redlich-Kwong-Soave (RK-SOAVE) thermodynamic model to calculate thermodynamic properties. The RK-SOAVE model is recommended for mixtures containing hydrocarbons and light gases and is suitable for estimating the thermodynamic properties of certain solids, including carbon (François *et al.* 2013). This model was employed to predict the physical properties

of both conventional mixed and non-conventional components. For non-conventional components, such as biomass, char, and ash, the enthalpy and density were calculated using the HCOALGEN and DCOALIGT models, respectively. The HCOALGEN model in Aspen Plus® requires three key attributes: proximate analysis (PROXANAL), ultimate analysis (ULTANAL), and sulfur analysis (SULFANAL). Ultimate analysis gives biomass or char mass composition in C, H, N, S, O, and ash. Proximate analysis reports the contents of MC, FC, VM, and ash. Finally, sulfur analysis divides the sulfur into pyritic and sulfate

Table 2. Reaction Rates for Homogeneous and Heterogeneous Reactions Involved in Char Oxidation

#	Gasification Reaction	Reaction Rate (mol/m^3·s))	Reference
Heterogeneous reaction			
R- 1	$C + \frac{Z+2}{2Z+2}O_2 \rightarrow \frac{z}{Z+1}CO + \frac{1}{Z+1}CO_2$	$\frac{P_{O_2}}{4.0\times10^5\left(1+\frac{1}{\varepsilon_b^{2.5}}\left(\frac{1}{Y}-1\right)\right)d_p}T^{0.75}$	(Al-Zareer *et al.* 2016; He *et al.* 2013; Wen and Chaung 1979)
R- 2	$C + H_2O \rightarrow CO + H_2$	$930e^{-\frac{22647}{T}}\left[c_C \times \left(P_{H_2O} - \left(3.23\times10^7\left(\frac{P_{H_2}\cdot P_{CO}}{e^{-\frac{16330}{T}}}\right)\right)\right)\right]$	(He *et al.* 2013; Wen and Chaung 1979)
R- 3	$C + CO_2 \rightarrow 2CO$	$930e^{-\frac{22647}{T}}\left[c_C \times \left(P_{CO_2} - \left(1.22\times10^9\left(\frac{{P_{CO}}^2}{e^{-\frac{20280}{T}}}\right)\right)\right)\right]$	(He *et al.* 2013)
R- 4	$C + 2H_2 \rightarrow CH_4$	$8.35\times10^{-4}e^{-\frac{8078}{T}}\left[c_C \times \left(P_{H_2} - \left({P_{H_2}}^* = \left(6.80\times10^5\frac{P_{CH_4}}{e^{-\frac{10100}{T}}}\right)^{0.5}\right)\right)\right]$	(Al-Zareer *et al.* 2016; He *et al.* 2013)
Homogeneous reaction			
R- 5	$H_2 + 0.5O_2 \rightarrow H_2O$	$8.83\times10^5e^{-\frac{11997}{T}[c_{H_2}\times c_{O_2}]}$	(Al-Zareer *et al.* 2016)

R- 6	$CH_4 + 2O_2 \rightarrow CO_2 + 2H_2O$	$3.55 \times 10^{11} e^{-\frac{11997}{T}} [c_{CH_4} \times c_{O_2}]$	(Al-Zareer *et al.* 2016; Xie *et al.* 2012)
R- 7	$CO + 0.5O_2 \rightarrow CO_2$	$6.36 \times 10^{3} e^{-\frac{11997}{T}} [c_{CO_2} \times c_{CO}]$	(Al-Zareer *et al.* 2016)
R- 8	$CO + H_2O \leftrightarrow CO_2 + H_2$	1: $2.78 \times 10^{3} e^{-\frac{1510}{T}}$ 2: $9.59 \times 10^{4} e^{-\frac{5609}{T}}$	(Rabea *et al.* 2022)
R- 9	$CH_4 + H_2O \leftrightarrow CO + 3H_2$	1: $6.09 \times 10^{14} e^{-\frac{30908}{T}}$ 2: $3.12 \times 10^{2} e^{-\frac{3608}{T}}$	(Rabea *et al.* 2022)
where c_C, c_{CH4} and c_{H2} are concentrations of C, CH_4 and H_2. P_{H2O}, P_{CO}, P_{CO2}, P_{H2} and P_{CH4} are partial pressure of components (atm). x_{CO}, x_{CO2}, and x_{H2} are mol fractions of components.			

Reaction kinetic of pyrolysis in the process simulation

The drying and devolatilization of biomass in the process simulation using Aspen Plus® can be modeled from the pyrolysis yields (Beheshti *et al.* 2015). In this approach, empirical correlations derived from experimental data are used. The pyrolysis reactions are presented below:

$$Dry\ biomass \rightarrow aChar + bH_2 + cCO + dCO_2 + eCH_4 + fH_2O_{(g)} + gC_xH_yO_z + hN_2 \quad (15)$$

The volatile matter produced includes CO, H_2, H_2O, CO_2, CH_4, N_2, and $C_xH_\gamma O\mathcal{z}$, where $C_xH_\gamma O\mathcal{z}$ represents condensable gases and tar as an empirical chemical compound. Two main approaches are commonly used to characterize pyrolysis products: experimental methods and theoretical models, such as functional group models **(**Hobbs *et al.* 1992**)**. The experimental approach was used in this study due to its simplicity and the availability of experimental data. The H_2O production was estimated based on the cellulose, hemicellulose, and lignin content, as analyzed by Stefanidis *et al*. (2014). The experimental data between 700 and 1000 °C yields were used to determine the coefficients of the Eq 15. In addition, the elemental compositions (carbon, hydrogen, and oxygen) of dry biomass and char under these conditions were used to balance the pyrolysis equation, allowing the determination of the empirical formula for char and $C_xH_\gamma O\mathcal{z}$ values. Table 3 presents the product yield balances obtained from the pyrolysis of AB at different temperatures.

Table 3. Product Mass Yields from Pyrolysis of AB at Different Temperatures

	Product Mass Yield (wt%)				
Component	700 °C	800 °C	900 °C	950 °C	1000 °C
CHAR	26.59	26.11	24.02	23.34	23.38
CO	3.64	5.28	7.22	8.27	8.46
H_2	0.35	0.31	0.66	0.64	0.75
CO_2	8.21	9.45	11.10	11.14	11.96
H_2O	24.00	24.00	24.00	24.00	24.00
H_2S	0.00	0.00	0.00	0.00	0.00
N_2	0.40	0.40	0.40	0.40	0.40
CH_4	0.88	1.03	1.03	0.98	0.98
$C_xH_\gamma O\mathcal{z}$	35.94	33.42	31.57	31.19	30.07

Process description and assumptions

The pyro-gasification process involves three main stages: drying, devolatilization (pyrolysis), and char oxidation. The stages were modeled in sequence. The flowchart modeled in Aspen Plus® is shown in Fig. 2. Briefly, the pyrolysis of biomasses was simulated with a RYield block (PYROLYS). This block decomposes the dry biomass into CO, H_2, CO_2, H_2O, N_2, CH_4, $C_xH_yO_z$, and char. The yield of each component is specified according to the experimental data. After pyrolysis, the products flow into the SEP-2 block to separate the pyrolysis gas and solid (char). The separator is configured as a split fraction separator, allowing the separation of gas-phase and solid-phase products based on their physical state. The gases from SEP-2 pass into a gas mixer (M-GAS). The char enters an RStoic model (CHAR-DEC) to decompose into its elemental components (C, H, O, N, and ash), according to the ultimate analysis of the char. For non-isothermal gasification, these elemental compounds pass through a series of plug flow reactor (PFRs) gasifiers operating at different temperatures, from 700 to 1000 °C, increasing in 50 °C for each reactor (RHETE-1 to RHETE-7) for heterogeneous reactions and (RHOMO-1 to RHOMO-7) for homogeneous reactions. For isothermal gasification, a stirred tank reactor (RCSTR) was used, with a residence time of 30 min. This reactor replaced the series of Plug Flow Reactors (PFRs) under isothermal conditions, ensuring the implementation of both homogeneous and heterogeneous reactions, as originally considered in the non-isothermal configuration. The details of each equipment are presented in Table 4.

Table 4. Details of Each Block and its Conditions

Block	Model	Function and Conditions
DRYING	RYield	Simulate biomass drying based on the value of the moisture content in the proximate analysis of biomass. The biomass with initial mass flow of 1500 kg/h.
PYROLYS	RYield	Simulate biomass pyrolysis based on the results data of pyrolysis experiment of biomasses
SEP-1 to SEP-3	SEP	The separator is configured as a split fraction separator, allowing the separation of gas-phase and solid-phase products based on their physical state.
CHAR-DEC	RStoic	Decompose char into its elemental components (C, H, O, N, and ash), according to the ultimate analysis
AIR-SEP	FSplit	Stream splitter. This separator was used to distribute the airflow equally to each reactor due to the non-isothermal condition of the process
MIX-1 to MIX-7	Mixer	This mixer combines the 'char' from the previous reactor with the airflow before entering the next reactor. It operates under the temperature and pressure conditions of the next reactor.
RHETE-1 to RHETE-7	RPlug	Simulation of heterogeneous gasification reactions (R1 to R4) was conducted using seven reactors, each operating at a different temperature ranging from 700 to 1000 ºC, with increments of 50 ºC per reactor. This approach was chosen to account for the non-isothermal nature of the gasification process.
SE-1 to SE-7	SSplit	Substream splitter (cyclone), this system allows the separation of solids, specifically char, from the reaction gases.
RHOMO-1 to RHOMO-7	RPlug	Simulation of homogeneous gasification reactions (R5 to R9) was conducted under the same conditions as the heterogeneous gasification, differing only in the reactions involved.
M-GAS	Mixer	Mix the product gas: Combines pyrolysis and gasification product gases along with the water vapor generated during drying.

In process modeling, several technical assumptions were considered:

- The process operates in a steady state.
- The reactor is assumed to be adiabatic.
- Non-condensable gases are limited to H_2, CH_4, CO, and CO_2.
- Char composition is modeled based on its ultimate carbon, hydrogen, nitrogen, oxygen, and ash content analysis.
- The gasifier system is considered a perfectly mixed environment.
- The operation is conducted at atmospheric pressure, with pressure drops in equipment neglected.
- Biomass drying and devolatilization (pyrolysis) are assumed to occur instantaneously at 700 °C for non-isothermal gasification and at 900 and 950 °C for isothermal gasification.
- NOx, HCN, and NH_3 concentrations were not taken into account; all biomass nitrogen is assumed to be inert (N_2).
- Pyrolysis product yields serve as initial conditions in the gasification step.

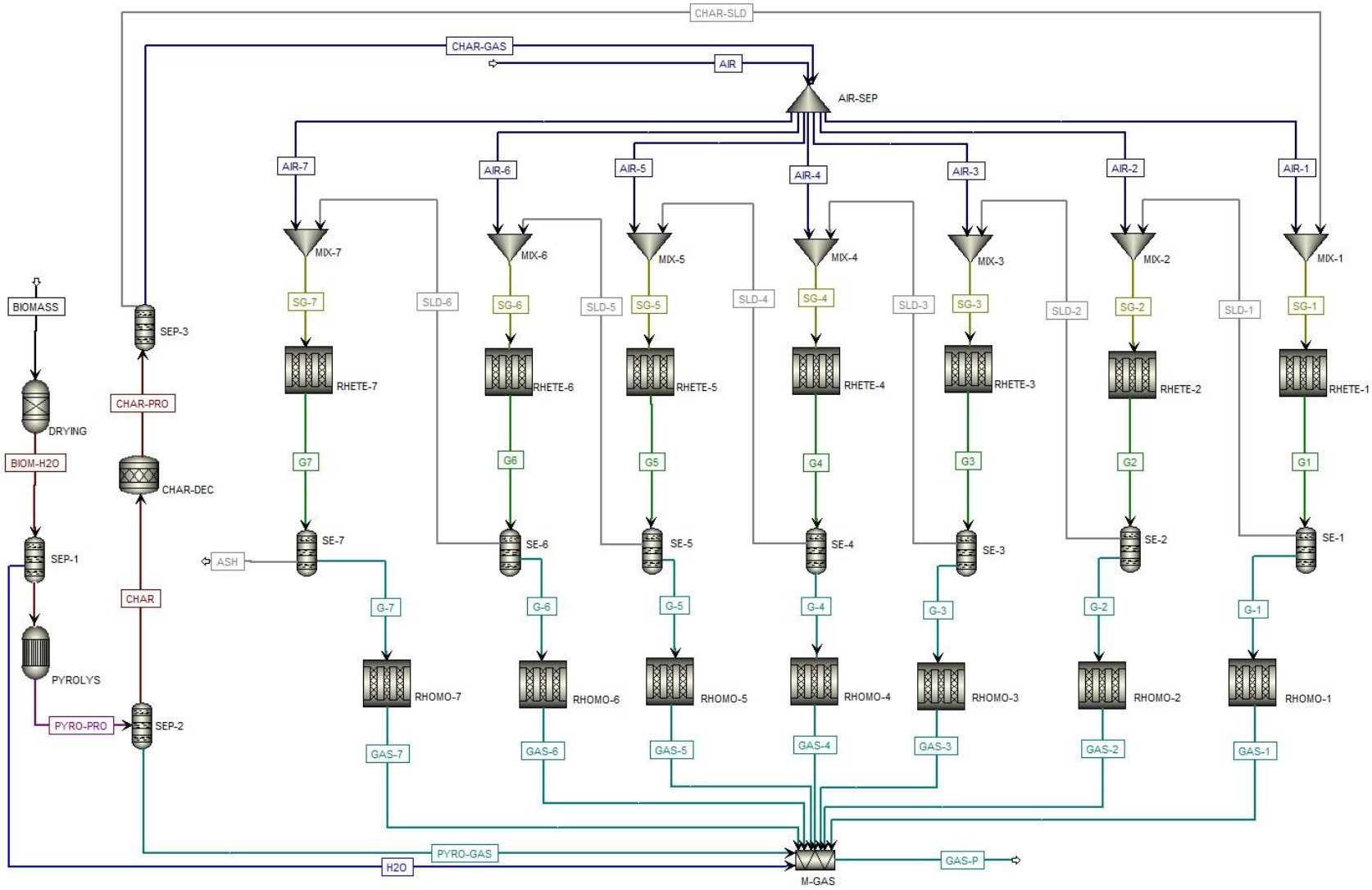

Fig. 2. Simulation model flowchart in Aspen Plus®

RESULTS AND DISCUSSION

Comparison of CFD Modeling and Process Simulation with Experimental Data

This section presents a comparative analysis of CFD modeling and process simulation results with experimental data for gasification processes. The analysis begins with non-isothermal gasification outcomes, followed by an examination of isothermal gasification results. The experimental data were replicated with a maximum error of 7% across all cases.

Non-isothermal gasification results

The results of non-isothermal gasification, derived from experimental analysis using TGA, were compared with predictions from CFD and SIM simulations. This comparative analysis aimed to assess the accuracy and predictive capabilities of the models across a range of ABR values (0.187 to 1). Experimental data served as a reference, emphasizing the influence of ABR on the yields of non-isothermal gasification products, including biochar, bio-oil, and non-condensable gases (NCG or biogas), within the temperature range of 700 to 1000 °C. The ABR in this study plays a role analogous to the equivalence ratio (ER), as commonly discussed in gasification studies (Beheshti *et al.* 2015; Torres *et al.* 2019), governing the oxygen availability relative to biomass and influencing the oxidation-reduction dynamics of the process. Figure 3 compares the overall product yields as a function of ABR variation.

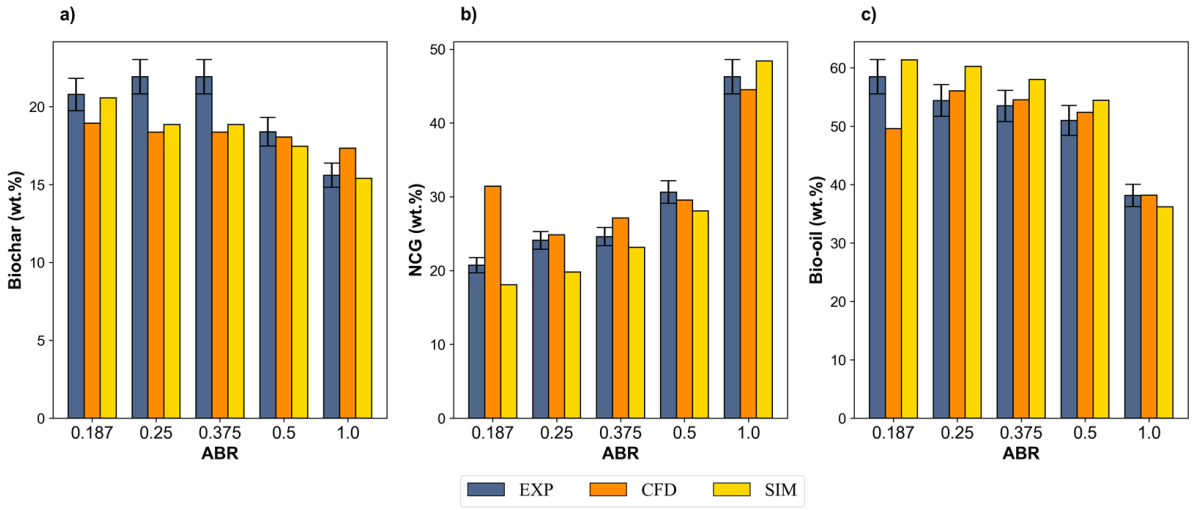

Fig. 3. Comparison of experimental and simulation results for the main products yields of non-isothermal gasification at ABR values: a) biochar, b) NCG, and c) Bio-oil

Both CFD and SIM exhibit deviations from experimental results, with the magnitude of these discrepancies varying based on the ABR. Figure 3a shows the comparison of biochar yield as a function of ABR. At low ABR values, such as 0.187, the SIM aligns closely with the experimental results, showing a minimal error of approximately 0.23 wt.%, whereas CFD slightly underestimates the biochar yield. However, as ABR increases, SIM overestimates the biochar yield, particularly at ABR = 0.375, where the error reaches 3.08 wt.%. In contrast, CFD consistently underestimates biochar yield across the entire ABR range, with the largest deviation observed at ABR = 0.375, reaching 3.55 wt.%. Both experimental and simulation results indicate that increasing ABR reduces biochar content, consistent with findings from non-isothermal gasification studies, where higher ABR values enhance oxidation intensity, reducing biochar yield (Torres *et al.* 2019).

The comparison of bio-oil yields indicates that the CFD model generally underestimates bio-oil yield at lower ABR values but aligns more closely with experimental data as ABR increases, as shown in Fig. 3b. For an ABR of 0.375, the prediction error of the CFD model was

1.04 wt.%, representing a better prediction under intermediate conditions. In contrast, the SIM model tends to overestimate the bio-oil yield at higher ABR value, with a notable maximum error of 5.87 wt.% at 0.25. This disparity highlights differences in how the models capture secondary reactions and product distributions.

The NCG yields (Fig. 3c) reveal distinct predictive behaviors for the two models across varying ABR values. At low ABR (e.g., 0.187), the CFD model significantly overestimates NCG yields, while the SIM model underestimates them. This contrast reflects differences in how the models handle reaction dynamics under oxidation conditions. As ABR increases, both models improve their agreement with experimental results. At ABR=0.375, the SIM model closely matches the experimental data, with an error of 1.44 wt.%, whereas the CFD model slightly overestimates yields, with an error of 2.52 wt.%. At the highest ABR (e.g., 1.0), the CFD model achieves near-perfect accuracy with an error of 1.77 wt.%, while the SIM model slightly underestimates NCG yields, with an error of 2.13 wt.%.

The analysis of individual non-condensable gases (H_2, CH_4, CO, and CO_2) shows discrepancies between experimental data and model predictions across all ABR values, as shown in Fig. 4.

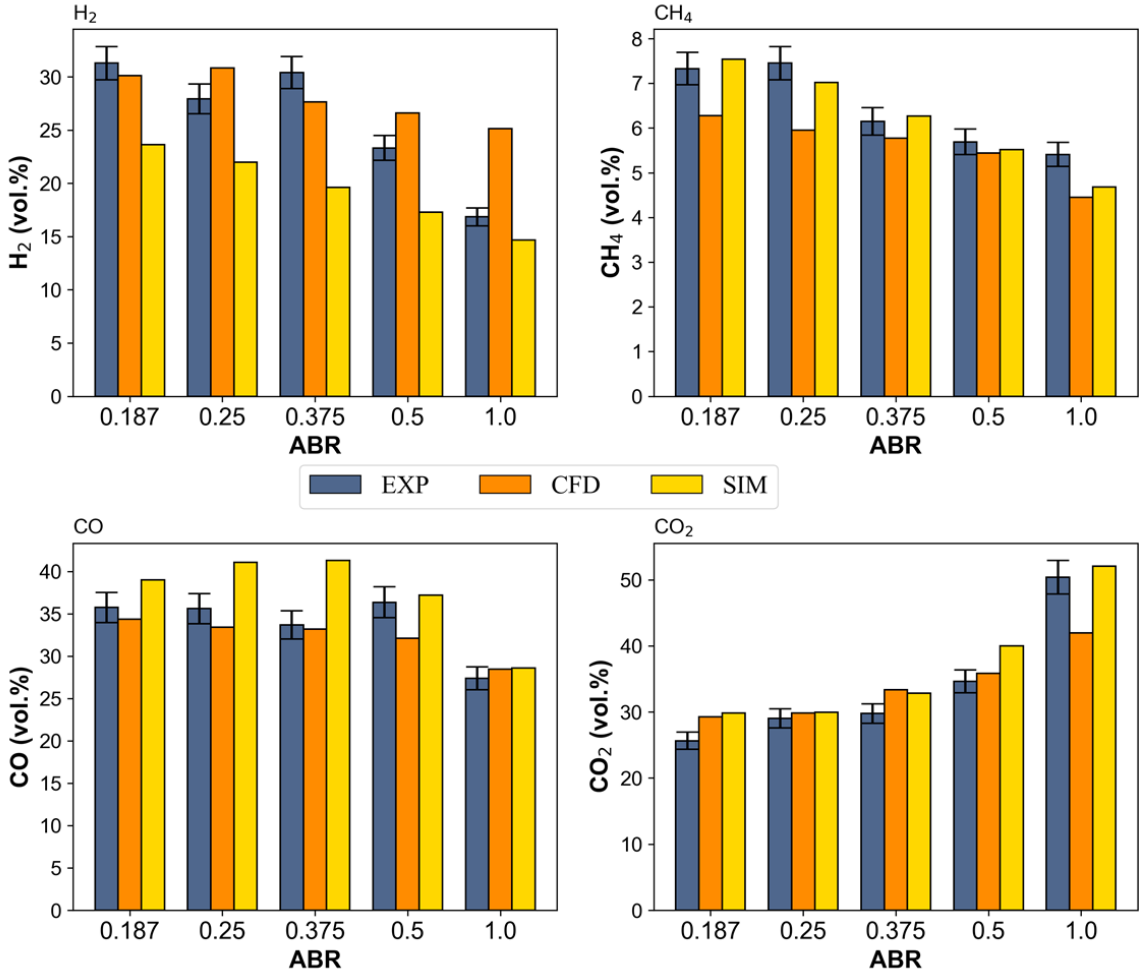

Fig. 4. Comparison of experimental and simulation results for the NCG composition of non-isothermal gasification

At low ABR (*e.g.*, 0.187), experimental results reveal higher H_2 and CO ratios, reflecting the dominance of partial oxidation and water-gas reactions. The CFD model accurately captures these trends, with an error of 1.05 wt.% for CO, but underestimates CH_4. In contrast, the SIM model exhibits larger deviations for H_2 and CO, with errors exceeding 7.67 wt.% in some cases. As ABR increases, reaction pathways shift, resulting in higher CO_2 production and reduced CO

and CH_4 ratios. Experimental data at ABR=0.375 shows a significant increase in CO_2, which the CFD model predicts well, with errors below 3.62 wt.%. However, the SIM model underestimates CO_2 at higher ABR values, overestimates CO, and consistently underpredicts H_2. Both models struggle with CH_4 predictions, consistently underestimating its composition, though the CFD model demonstrates slightly better alignment than the SIM model.

Under non-isothermal conditions (700 to 1000 °C) and varying ABR (0.187 to 1), both models demonstrate significant predictive capabilities but show specific limitations. The SIM model exhibits greater accuracy in predicting global products, such as biochar, bio-oil, and NCG (gases), which can be attributed to its continuous-system approach and ability to capture general trends. However, certain discrepancies in the prediction of non-condensable gas compositions, such as H_2, CH_4, CO, and CO_2, indicate that the model would require refinements in its kinetic description and aspects of thermodynamic models to better represent the phase equilibria under non-isothermal conditions studied.

In contrast, the CFD model provides more accurate predictions of the non-condensable gas composition, better representing the thermochemical dynamics of the reactor, including reaction kinetics and heat transfer phenomena. However, discrepancies in the overall product yields were observed, suggesting the need for further refinement in modeling under these conditions.

The comparative analysis showed the complementary strengths of both models. While the SIM model better predicts overall product trends, the CFD model better predicts gas composition. This suggests that a hybrid modeling approach, which takes advantage of the strengths of both frameworks, could significantly improve the accuracy of predictions for non-isothermal gasification processes.

Isothermal Gasification Results

Figure 5 presents the comparison between experimental data and predicted values. The results reveal that both CFD and SIM consistently overestimate biochar yields compared to experimental data. At 900 °C, the CFD model overpredicts by 7.24 wt.%, decreasing slightly to 6.04 wt.% at 950 °C. Conversely, SIM exhibits more moderate overestimations, with differences of 3.6 w.% at 900 °C and 2.51 wt.% at 950 °C.

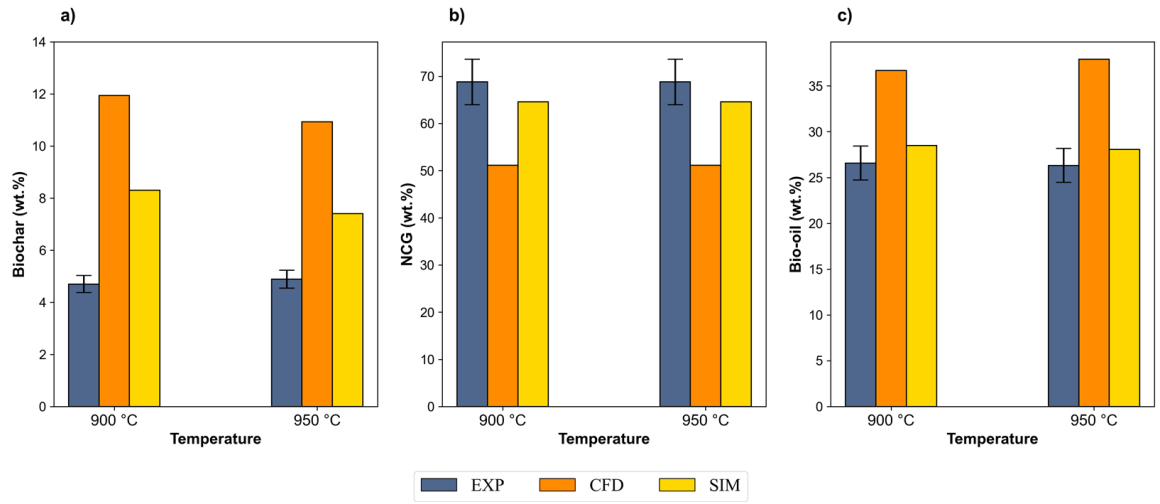

Fig. 5. Comparison of experimental and simulation results for the main products yields of isothermal gasification

Both models overestimate the experimental results for bio-oil. At 900 °C, the CFD model predicts a yield of 36.67 wt.%, exceeding the experimental value by 10.09 wt.%. This discrepancy increases to 11.59 wt.% at 950 °C. In contrast, SIM achieves better accuracy with deviations of 1.89 wt.% and 1.72 wt.% at 900 °C and 950 °C, respectively.

In the case of NCG, both models underestimate experimental yields. The CFD

significantly underpredicts with differences exceeding 17 wt.% for both temperatures. While still underestimating, SIM exhibits smaller deviations of 5.49 wt.% at 900 °C and 4.24 wt.% at 950 °C. Overall, the models overestimate biochar and bio-oil yields while significantly underestimating NCG. SIM aligns more closely with experimental data across all product types, whereas CFD exhibits more significant deviations, particularly in gas-phase reactions. Both models perform slightly better at higher temperatures (950 °C) but require further refinement for improved accuracy. Figure 6 shows that the analysis of gas compositions reveals distinct differences between experimental data and the predictions of CFD and SIM models at 900 and 950 °C.

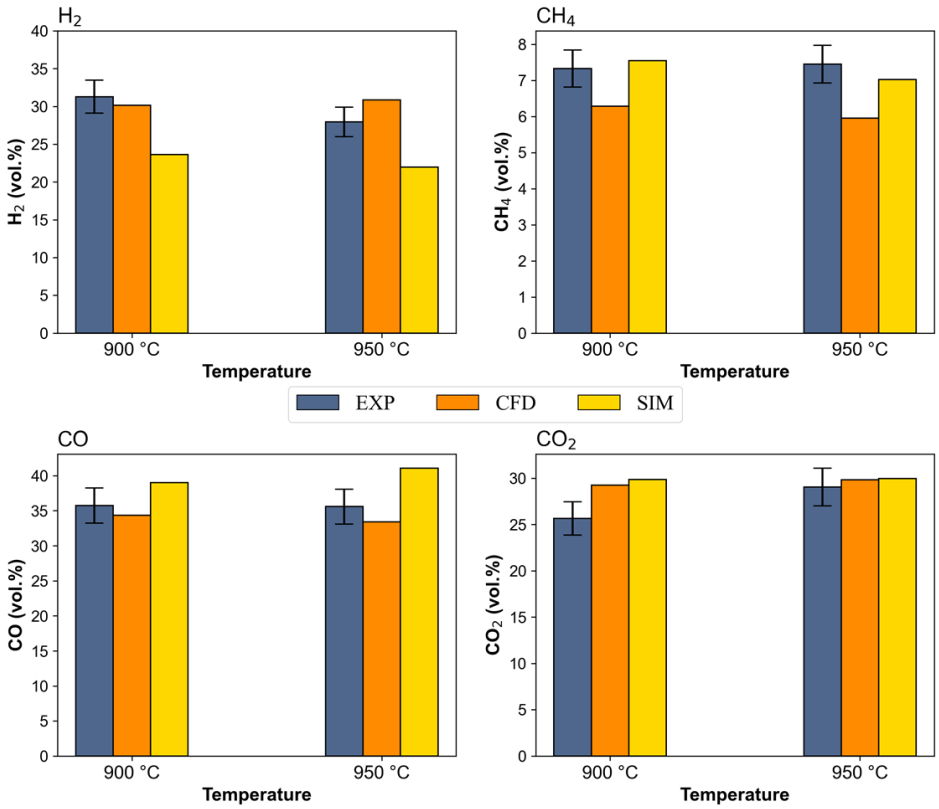

Fig. 6. Comparison of experimental and simulation results for NCG composition of isothermal gasification

At 900 °C, both models follow similar trends, slightly overestimating H_2, CH_4, and CO while underestimating CO_2. For H_2, the CFD model shows a deviation of 3.71 vol.%, whereas SIM demonstrates more accurate predictions with a smaller difference of 0.7 vol.%. Both models demonstrated minimal differences for CH_4, with CFD deviating by 0.66 vol.% and SIM by 0.32 vol.%. For CO, CFD overestimates by 4.85 vol.%, while SIM shows a smaller difference of 3.24 vol.%. For CO_2, both models underestimate its content, with CFD showing a difference of 9.22 vol.% compared to 4.26 vol.% for SIM.

At 950 °C, the CFD model slightly overestimates H_2 content, with a deviation of 2.55 vol.%, while SIM achieves greater accuracy, showing a difference of only 0.52 vol.%. For CH_4, both models agree better with the experimental data, with differences of less than 0.8 vol.%. For CO, CFD underestimates the content by 2.98 vol.%, whereas SIM shows a smaller difference of 0.82 vol.%. Finally, for CO_2, both models achieve highly accurate predictions, with differences below 0.5 vol.%. Overall, SIM demonstrates better alignment with experimental data, particularly for H_2 and CO at 950 °C, while CFD exhibits greater variability, especially at 900 °C, where it overestimates H_2 and CO. Both models' persistent underestimation of CO_2 suggests a need for refining the kinetic dynamics under gasification conditions.

Although both models underestimate certain yields (biochar and bio-oil) under non-isothermal gasification conditions, SIM generally agrees better with experimental data for overall product yields. However, the CFD model excels in predicting gas compositions, reflecting its ability to capture the dynamics of specific reactions, particularly under non-equilibrium conditions, where temperature gradients may exist in the reactor. Under isothermal gasification conditions, where the system approaches thermal equilibrium, the SIM model accurately predicts overall product yields and gas compositions, consistent with its thermodynamic equilibrium-based assumptions.

Sensitivity Analysis of Isothermal Gasification Processes

The sensitivity analysis of isothermal gasification was conducted using CFD modeling and process simulations to evaluate the impact of the key parameters: (i) the isothermal gasification temperature, from 700 to 1500 °C; and (ii) the ABR values between 1 and 2.5. These factors were analyzed to determine their influence on the overall products yields in the process and the composition of the produced.

Effect of ABR and temperature on overall products yields

The yields of the main products —biochar, bio-oil, and NCG— are significantly influenced by temperature and ABR, as illustrated in Figs. 7 through 9. Biochar, as shown in Fig. 7, decreases progressively with increasing temperature. This reduction is attributed to the activation of heterogeneous reactions in the solid phase, particularly carbon oxidation (R- 1) (Al-Zareer *et al.* 2016; He *et al.* 2013; Wen and Chaung 1979) and the Boudouard reaction (R-3) (He *et al.* 2013). These endothermic reactions are favored at higher temperatures. Incomplete carbon conversion results in higher biochar yields at lower temperatures and ABR values. However, oxygen availability promotes oxidation as the ABR increases, accelerating biochar conversion into gases. In this context, CFD and SIM simulations exhibit similar trends, though CFD predicts higher biochar yields and a more gradual decline than SIM. This emphasizes the influence of modeling approaches on product distribution.

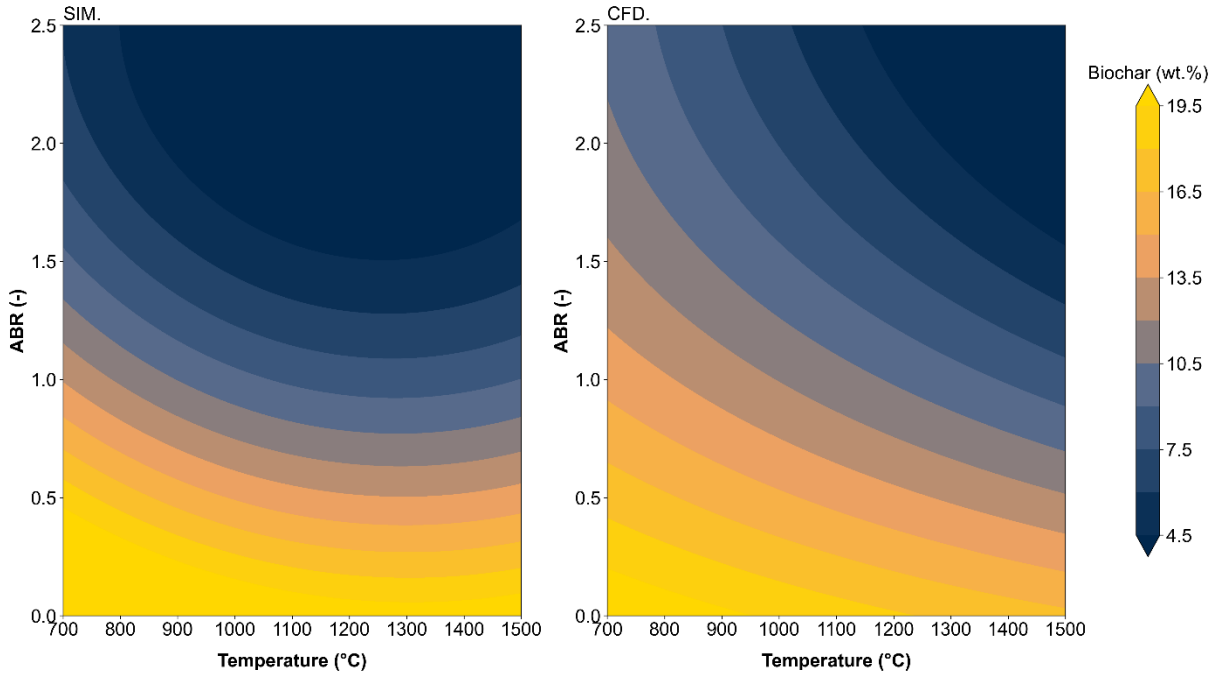

Fig. 7. Effect of ABR and temperature on biochar yield: SIM and CFD comparison

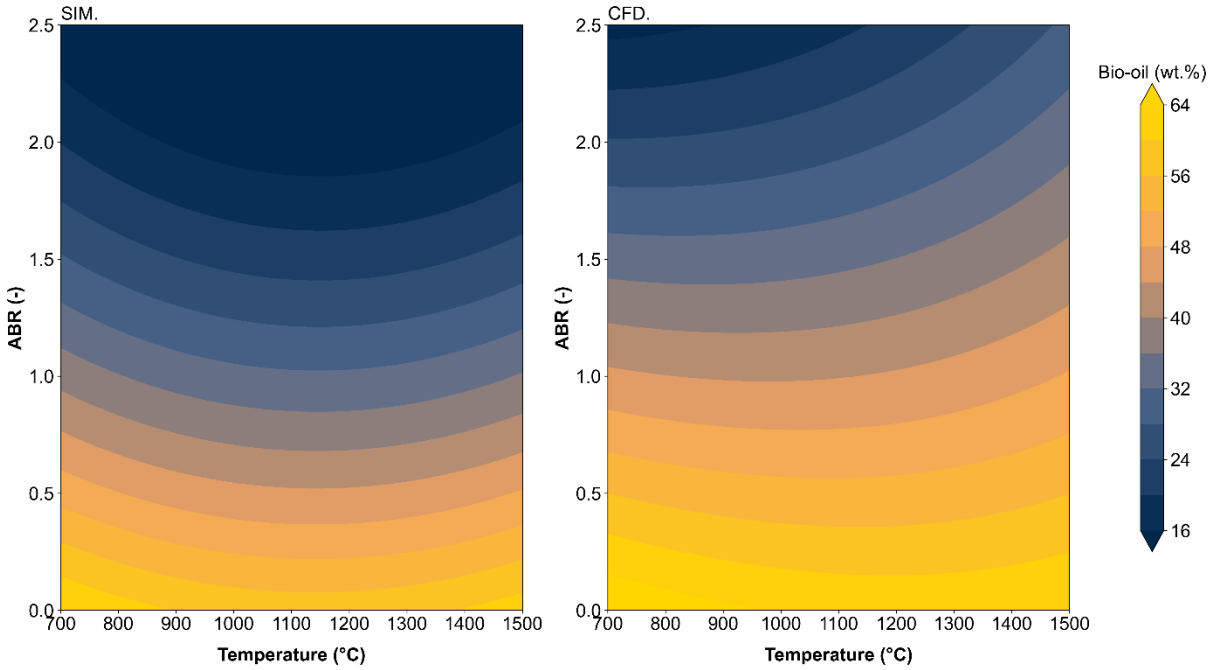

Fig. 8. Effect of ABR and temperature on bio-oil yield: SIM and CFD comparison

Bio-oil, primarily comprising condensable gas products and water vapor, is influenced by temperature and ABR, as shown in Fig. 8. During pyrolysis, biomass undergoes thermal decomposition, releasing vapors that condense into bio-oil. As the temperature increases, these vapors undergo secondary reactions, such as steam reforming and thermal cracking, promoting the formation of non-condensable gases (Sangaré *et al.* 2024b; Zhu *et al.* 2018). Additionally, during gasification, increased ABR enhances biochar oxidation through oxygen supply, further decreasing bio-oil production. The CFD and SIM models exhibit similar trends, but CFD predicts a more gradual decrease in bio-oil yield, whereas SIM shows an abrupt decline, indicating distinct modeling behaviors under similar conditions.

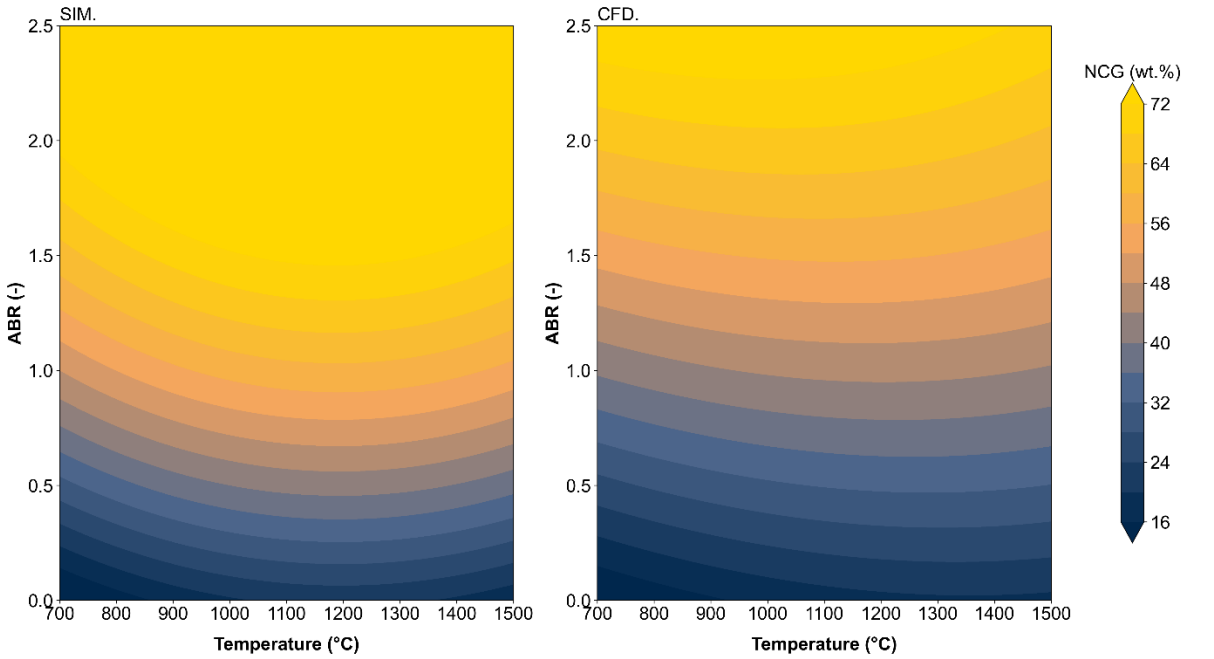

Fig. 9. Effect of ABR and temperature on NCG yield: SIM and CFD comparison

The yields of NCG, including H_2, CH_4, CO, and CO_2, increase significantly with the increasing temperature and ABR, as shown in Fig. 9. This is due to the dominant role of heterogeneous reactions (R- 1 to R- 4) (He *et al.* 2013; Al-Zareer *et al.* 2016). At low ABR values and high temperatures, limited oxidation favors the production of combustible gases such as H_2 and CO. However, as ABR increases, homogeneous oxidation reactions become more prominent, leading to a higher proportion of CO_2 (Jangsawang *et al.* 2015), increased overall yields, and reduced proportions of combustible gases. The CFD and SIM models exhibit similar trends, but their distributions differ: the SIM model predicts higher and more uniform NCG yields with increasing ABR, while the CFD model shows lower yields under similar conditions.

Overall, the observed differences between CFD and SIM predictions highlight the influence of model assumptions on phase interactions and reaction dynamics. CFD offers a detailed perspective by explicitly accounting for heterogeneous and homogeneous phase reactions, while the SIM equilibrium-based approach results in a more uniform phase distribution.

Effect of ABR and temperature on gas composition

The effects of ABR and temperature on gas composition are presented in Figs. 10 through 13. As depicted in Fig. 10, the volumetric fraction of H_2 consistently increases with temperature in both models, reflecting the endothermic nature of heterogeneous gasification reaction (R- 2).

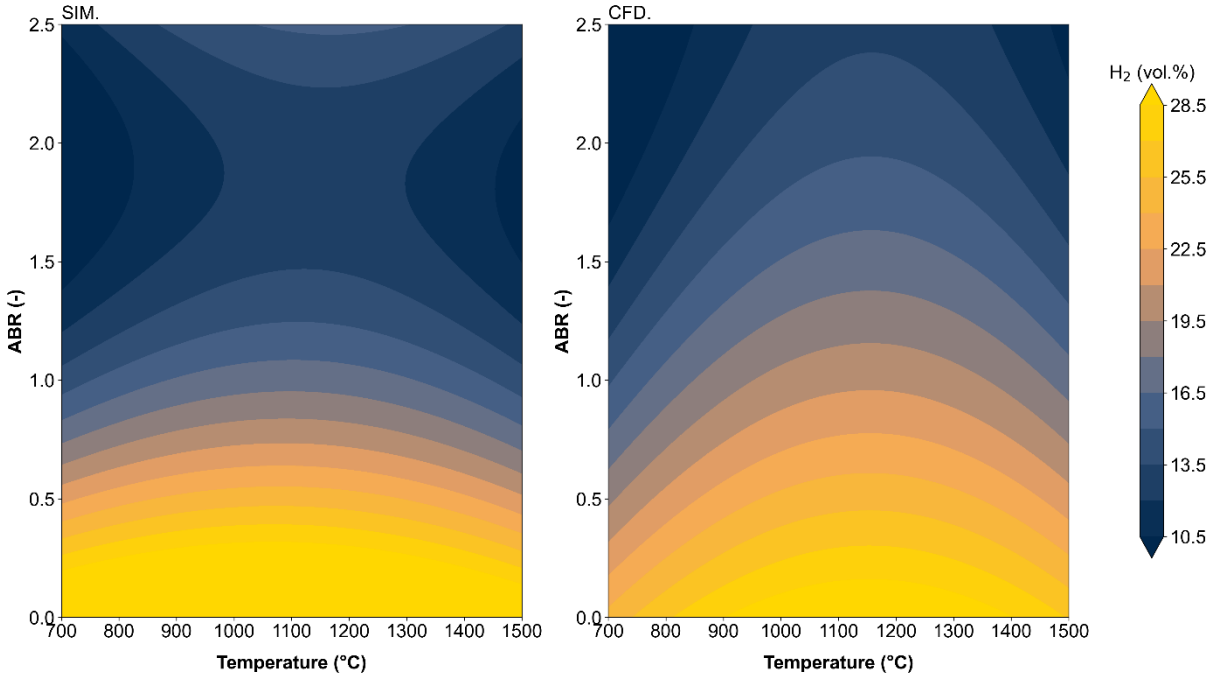

Fig. 10. Effect of ABR and temperature on H_2 composition: SIM and CFD comparison

This reaction predominantly occurs on the solid surface and is facilitated by increased thermal energy, resulting in greater H_2 production. Under low ABR conditions, where oxygen availability is limited, H_2 reaches its maximum concentration as homogeneous oxidation reactions, such as R- 5, are constrained. Conversely, at higher ABR values, H_2 is consumed in oxidation reactions to produce water vapor, reducing its concentration. This phenomenon, as described by Kumar and Paul (2020), underscores the sensitivity of these endothermic reactions to temperature changes and their influence on gas composition during gasification process. Both heterogeneous and homogeneous reactions contribute to H_2 production, yielding similar trends across the two models.

The evolution of H_2 is directly linked to the behavior of CH_4, as shown in Fig. 11. At low temperatures, CH_4 formation is dominated by the heterogeneous methanation reaction (R-

4), where solid carbon reacts with H_2 in an exothermic. However, as the temperature increases, CH_4 undergoes decomposition via steam reforming (R- 9), an endothermic reaction that generates H_2 and CO. Notably, most of the CH_4 in the gas mixture originates from pyrolysis. In both models, CH_4 concentrations decrease with increasing ABR, as oxygen promotes oxidation, which constrains CH_4 formation. Furthermore, high temperatures lead to a slight reduction in CH_4, particularly in the SIM results, due to enhanced gas-phase reaction reforming reaction (R-9). However, the CFD model predicts higher CH_4 concentrations than the SIM results, especially at high temperatures and low ABR values.

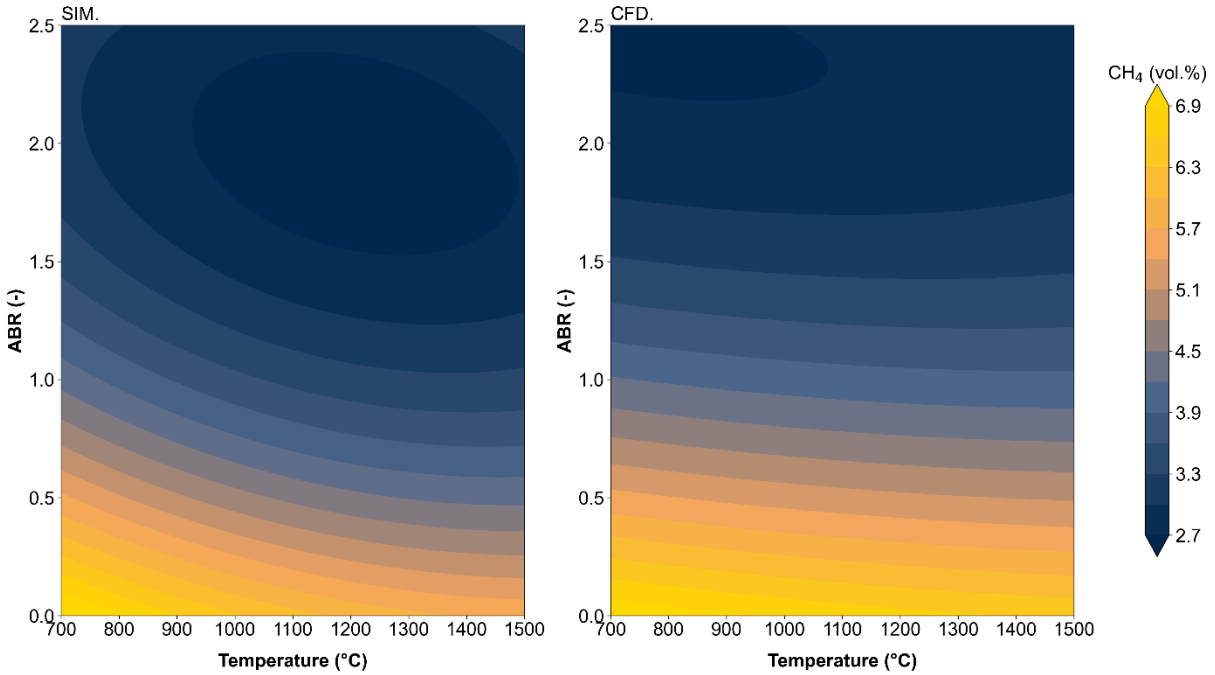

Fig. 11. Effect of ABR and temperature on CH_4 composition: SIM and CFD comparison

The behavior of CO, shown in Fig. 12, highlights the important role of heterogeneous reactions such as the partial oxidation of solid carbon (R- 1), which produces CO and CO_2. The Z coefficient in Eq. 14 regulates this reaction, increasing with temperature and favoring CO production at low ABR values. As the temperature increases, the Boudouard reaction (R- 3) and the steam reaction (R- 2) dominate, converting CO_2 and water vapor into CO and H_2. These heterogeneous reactions are key drivers of CO formation (Kumar and Paul 2020). However, at high ABR values, homogeneous oxidation reactions (R- 7) consume CO at high ABR values, reducing its concentration. While the CFD model better captures localized surface interactions, the SIM results align well with theoretical expectations, particularly at high temperatures and ABR values, which is likely due to its representation of the homogeneous CO oxidation reaction (R- 7).

CO formation is predominantly driven by heterogeneous reactions in the solid phase, whereas CO_2 production is mainly associated with homogeneous reactions, such as CO oxidation (R- 7), CH_4 combustion (R- 6), and the Water-Gas Shift reaction (R- 8) at lower temperatures (Jangsawang *et al.* 2015). Figure 13 illustrates the interactions of ABR and temperature on CO_2 composition.

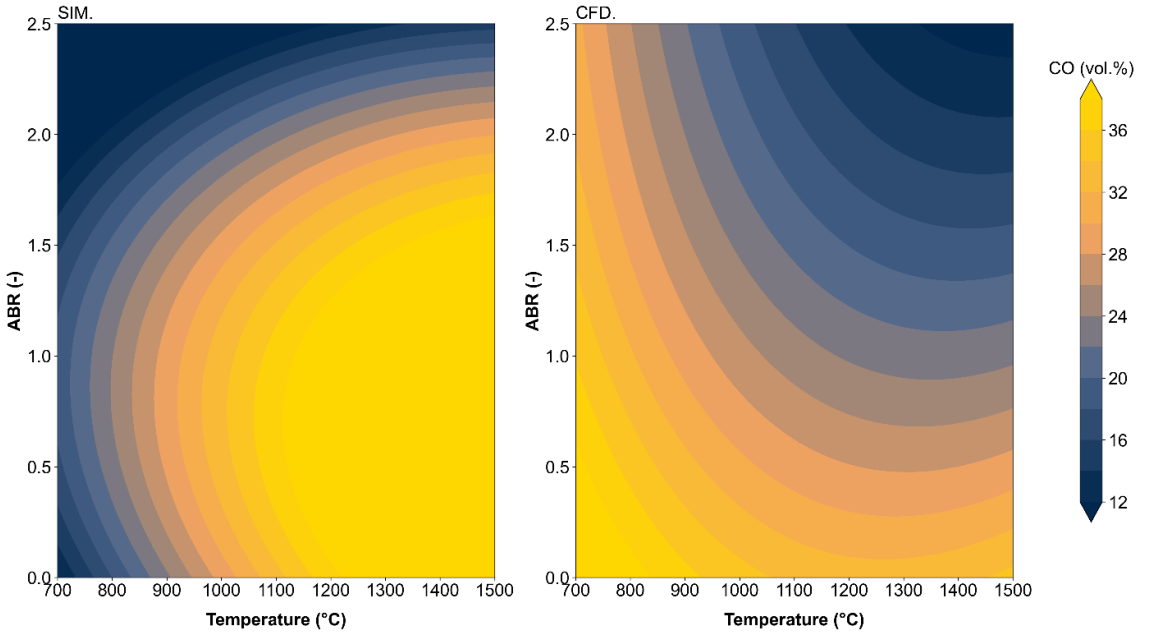

Fig. 12. Effect of ABR and temperature on CO composition: SIM and CFD comparison

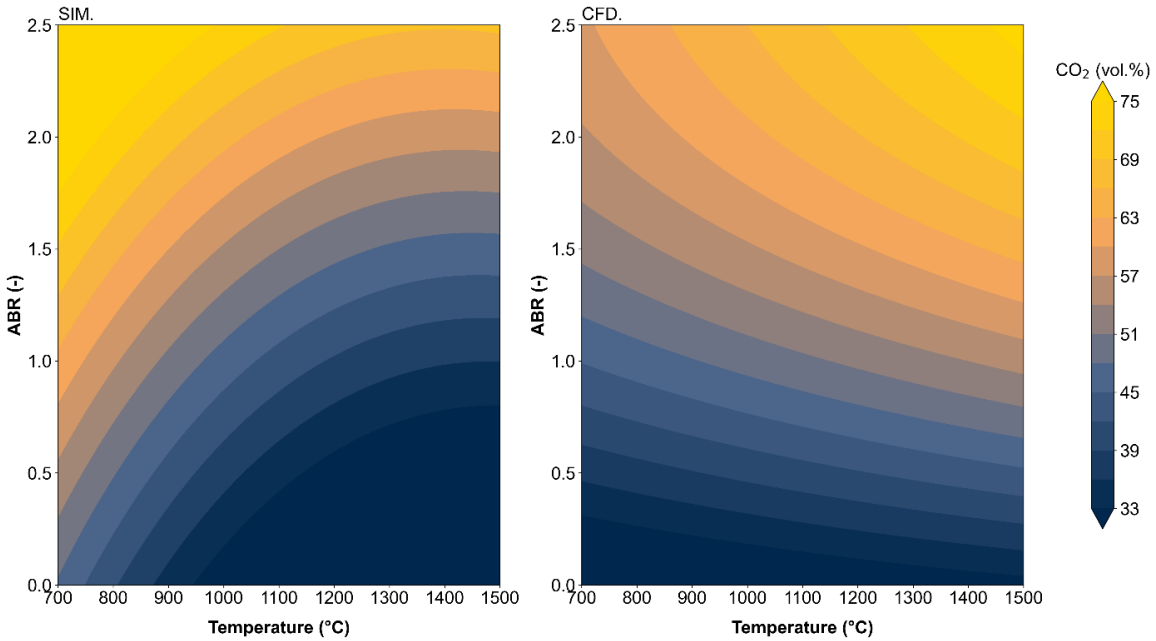

Fig. 13. Effect of ABR and temperature on CO_2 composition: SIM and CFD comparison

Theoretically, CO_2 production is favored at low temperatures and high ABR due to the increased availability of oxygen, promoting oxidation reactions. However, CO_2 is consumed at higher temperatures via the Boudouard reaction (R- 3), resulting in its progressive decrease in high-temperature, low ABR conditions. Figure 13 also reveals differences between CFD and SIM predictions. The CFD model shows higher values for CO_2 concentrations compared to the SIM results, particularly at higher ABR and temperatures. This discrepancy may be linked to homogeneous reactions. Ajorloo et al. (2022) emphasize the significance of homogeneous reactions in determining CO_2 distribution. The CFD model explicitly separates heterogeneous reactions in the solid phase from homogeneous reactions in the gas phase, whereas the SIM model assumes a uniform distribution of solids and gases throughout the reactor. These differences in phase representation may lead to variations in how phase interactions and reaction dynamics are modeled.

In summary, the formation of H_2 and CH_4 primarily arises from heterogeneous reactions, with both models showing similar trends. In contrast, while CO is mainly generated through heterogeneous reactions, it is subsequently consumed during homogeneous reactions to form CO_2. The discrepancies in CO and CO_2 trends between the models likely stem from differences in the treatment of homogeneous reactions, particularly CO oxidation, and the representation of phase interactions in each modeling approach.

CONCLUSIONS

1. This study has provided a detailed comparative analysis of computational fluid dynamics (CFD) and process simulation (SIM) approaches for modeling biomass pyro-gasification, supported by experimental data from agave bagasse. The findings emphasize the complementary strengths of these methodologies. Indeed, concerning modeling performance and applicability, CFD proved superior for non-isothermal conditions (700 to 1000 °C), accurately capturing heat and mass transfer dynamics and localized reactions, which are critical for understanding reactor behavior under temperature gradients, while SIM demonstrated better alignment with experimental yields under isothermal conditions (900 to 950 °C), where equilibrium-based models provide reliable predictions.
2. Sensitivity analysis showed the influence of temperature and ABR on overall product yield distributions and non-condensable gas compositions, demonstrating how these parameters can be used to optimize syngas production. Furthermore, the results underline the importance of selecting modeling methods based on process conditions.
3. For instance, CFD is highly suitable for reactors with thermal gradients, while SIM offers reliable performance in systems operating at near-equilibrium conditions. A hybrid modeling approach combining the detailed insights of CFD with the scalability of SIM could facilitate the development of more efficient biomass conversion technologies.
4. By leveraging the complementary capabilities of CFD and SIM, researchers and industry practitioners can address critical challenges in biomass pyro-gasification, accelerating the development of sustainable and efficient energy solutions.

ACKNOWLEDGMENTS

The authors express their gratitude to CONACYT (Consejo Nacional de Ciencia y Tecnología de México) for awarding scholarship No. 659624, which provided essential support for this research. We also acknowledge CIRAD-BioWooEB teams (France) for their technical support and the loan of equipment used in the analyses. Additionally, we thank ICARE-CNRS (France) for providing laboratory equipment and technical assistance, as well as the Région Centre-Val de Loire for financial support through the FITe federation.

REFERENCES CITED

Ajorloo, M., Ghodrat, M., Scott, J., and Strezov, V. (2022). "Recent advances in thermodynamic analysis of biomass gasification: A review on numerical modelling and simulation," *Journal of the Energy Institute* 102, 395-419. DOI: 10.1016/j.joei.2022.05.003

Al-Zareer, M., Dincer, I., and Rosen, M. A. (2016). "Effects of various gasification parameters and operating conditions on syngas and hydrogen production," *Chemical*

Engineering Research and Design 115, 1-18. DOI: 10.1016/j.cherd.2016.09.009

Ascher, S., Watson, I., and You, S. (2022). "Machine learning methods for modelling the gasification and pyrolysis of biomass and waste," *Renewable and Sustainable Energy Reviews* 155, article 111902. DOI: 10.1016/j.rser.2021.111902

Basu, P. (2018). *Biomass Gasification, Pyrolysis and Torrefaction: Practical Design and Theory*, Academic Press, Cambridge, MA, USA.

Bear, J., and Braester, C. (1972). "On the flow of two immscible fluids in fractured porous media," in: *Developments in Soil Science*, Vol. 2, Elsevier, pp. 177-202. DOI: 10.1016/s0166-2481(08)70538-5

Beheshti, S., Ghassemi, H., and Shahsavan-Markadeh, R. (2015). "Process simulation of biomass gasification in a bubbling fluidized bed reactor," *Energy Conversion and Management* 94, 345-352. DOI: 10.1016/j.enconman.2015.01.060

Debiagi, P. E. A., Pecchi, C., Gentile, G., Frassoldati, A., Cuoci, A., Faravelli, T., and Ranzi, E. (2015). "Extractives extend the applicability of multistep kinetic scheme of biomass pyrolysis," *Energy & Fuels* 29(10), 6544-6555. DOI: 10.1021/acs.energyfuels.5b01753

Devi, L., Ptasinski, K. J., Janssen, F. J., van Paasen, S. V., Bergman, P. C., and Kiel, J. H. (2005). "Catalytic decomposition of biomass tars: Use of dolomite and untreated olivine," *Renewable Energy* 30(4), 565-587. DOI: 10.1016/j.renene.2004.07.014

Elorf, A., Kandasamy, J., Belandria, V., Bostyn, S., Sarh, B., and Gökalp, I. (2019). "Heating rate effects on pyrolysis, gasification and combustion of olive waste," *Biofuels* 1-8. DOI: 10.1080/17597269.2019.1594598

Fatehi, H., Weng, W., Costa, M., Li, Z., Rabaçal, M., Aldén, M., and Bai, X.-S. (2019). "Numerical simulation of ignition mode and ignition delay time of pulverized biomass particles," *Combustion and Flame* 206, 400-410. DOI: 10.1016/j.combustflame.2019.05.020.

François, J., Abdelouahed, L., Mauviel, G., Patisson, F., Mirgaux, O., Rogaume, C., Rogaume, Y., Feidt, M., and Dufour, A. (2013). "Detailed process modeling of a wood gasification combined heat and power plant," *Biomass and Bioenergy* 51, 68-82. DOI: 10.1016/j.biombioe.2013.01.004

Gao, X., Zhang, Y., Li, B., and Yu, X. (2016a). "Model development for biomass gasification in an entrained flow gasifier using intrinsic reaction rate submodel," *Energy Conversion and Management* 108, 120-131. DOI: 10.1016/j.enconman.2015.10.070

Gao, X., Zhang, Y., Li, B., Zhao, Y., and Jiang, B. (2016b). "Determination of the intrinsic reactivities for carbon dioxide gasification of rice husk chars through using random pore model," *Bioresource Technology* 218, 1073-1081. DOI: 10.1016/j.biortech.2016.07.057

Gmehling, J., Kleiber, M., Kolbe, B., and Rarey, J. (2019). *Chemical Thermodynamics for Process Simulation*, Wiley, Hoboken, NJ, USA.

Guizani, C., Louisnard, O., Sanz, F.E., and Salvador, S. (2015). "Gasification of woody biomass under high heating rate conditions in pure CO2: Experiments and modelling," *Biomass and Bioenergy* 83, 169-182. DOI: 10.1016/j.biombioe.2015.09.017

Guo, L., Jin, H., and Lu, Y. (2015). "Supercritical water gasification research and development in China," *The Journal of Supercritical Fluids* 96, 144-150. DOI: 10.1016/j.supflu.2014.09.023

He, C., Feng, X., and Chu, K. H. (2013). "Process modeling and thermodynamic analysis of Lurgi fixed-bed coal gasifier in an SNG plant," *Applied Energy* 111, 742-757. DOI: 10.1016/j.apenergy.2013.05.045

Hobbs, M. L., Radulovic, P. T., and Smoot, L. D. (1992). "Modeling fixed-bed coal gasifiers," *AIChE Journal* 38(5), 681-702.

Jangsawang, W., Laohalidanond, K., and Kerdsuwan, S. (2015). "Optimum equivalence ratio of biomass gasification process based on thermodynamic equilibrium model," *Energy Procedia* 79, 520-527. DOI: 10.1016/j.egypro.2015.11.528

Jayaraman, K., and Gökalp, I. (2015). "Pyrolysis, combustion and gasification characteristics of miscanthus and sewage sludge," *Energy Conversion and Management* 89, 83-91. DOI: 10.1016/j.enconman.2014.09.058

Kumar, U., and Paul, M. C. (2020). "Sensitivity analysis of homogeneous reactions for thermochemical conversion of biomass in a downdraft gasifier," *Renewable Energy* 151, 332-341. DOI: 10.1016/j.renene.2019.11.025.

Li, C., and Suzuki, K. (2009). "Tar property, analysis, reforming mechanism and model for biomass gasification—An overview," *Renewable and Sustainable Energy Reviews* 13(3), 594-604. DOI: 10.1016/j.rser.2008.01.009

Li, S., Xu, S., Liu, S., Yang, C., and Lu, Q. (2004). "Fast pyrolysis of biomass in free-fall reactor for hydrogen-rich gas," *Fuel Processing Technology* 85(8-10), 1201-1211. DOI: 10.1016/j.fuproc.2003.11.043.

Lin, Y., Yan, W., and Sheng, K. (2016). "Effect of pyrolysis conditions on the characteristics of biochar produced from a tobacco stem," *Waste Management & Research* 34(8), 793-801. DOI: 10.1177/0734242x16654977

Liu, Q., Chmely, S. C., and Abdoulmoumine, N. (2017). "Biomass treatment strategies for thermochemical conversion," *Energy & Fuels* 31(4), 3525-3536. DOI: 10.1021/acs.energyfuels.7b00258

Mermoud, F., Golfier, F., Salvador, S., Van de Steene, L., and Dirion, J.-L. (2006). "Experimental and numerical study of steam gasification of a single charcoal particle," *Combustion and Flame* 145(1-2), 59-79. DOI: 10.1016/j.combustflame.2005.12.004.

Millington, R., and Quirk, J. (1961). "Permeability of porous solids," *Transactions of the Faraday Society* 57, 1200-1207. DOI: 10.1039/tf9615701200.

Moghadam, R. A., Yusup, S., Azlina, W., Nehzati, S., and Tavasoli, A. (2014). "Investigation on syngas production via biomass conversion through the integration of pyrolysis and air–steam gasification processes," *Energy Conversion and Management* 87, 670-675. DOI: 10.1016/j.enconman.2014.07.065

Nguyen, H. N., Van De Steene, L., and Le, D. D. (2018). "Kinetics of rice husk char gasification in an H_2O or a CO_2 atmosphere," *Energy Sources, Part A: Recovery, Utilization, and Environmental Effects* 40(14), 1701-1713. DOI: 10.1080/15567036.2018.1486900.

Niu, M., Huang, Y., Jin, B., and Wang, X. (2014). "Oxygen gasification of municipal solid waste in a fixed-bed gasifier," *Chinese Journal of Chemical Engineering* 22(9), 1021-1026. DOI: 10.1016/j.cjche.2014.06.026

Nsaful, F., Görgens, J., and Knoetze, J. (2013). "Comparison of combustion and pyrolysis for energy generation in a sugarcane mill," *Energy Conversion and Management* 74, 524-534. DOI: 10.1016/j.enconman.2013.07.024

Okoro, N., Harding, K., and Daramola, M. (2020). "Pyro-gasification of invasive plants to syngas," in: *Valorization of Biomass to Value-Added Commodities*, Springer, Amsterdam, pp. 317-340. DOI: 10.1007/978-3-030-38032-8_16

Okoro, O. V., Sun, Z., and Birch, J. (2017). "Meat processing waste as a potential feedstock for biochemicals and biofuels–A review of possible conversion technologies," *Journal of Cleaner Production* 142, 1583-1608. DOI: 10.1016/j.jclepro.2016.11.141

Patra, T. K., and Sheth, P. N. (2015). "Biomass gasification models for downdraft gasifier: A state-of-the-art review," *Renewable and Sustainable Energy Reviews* 50, 583-593. DOI: 10.1016/j.rser.2015.05.012.

Rabea, K., Michailos, S., Akram, M., Hughes, K.J., Ingham, D., and Pourkashanian, M. (2022). "An improved kinetic modelling of woody biomass gasification in a downdraft reactor based on the pyrolysis gas evolution," *Energy Conversion and Management* 258, artcle 115495. DOI: 10.1016/j.enconman.2022.115495.

Safarian, S., Unnþórsson, R., and Richter, C. (2019). "A review of biomass gasification

modelling," *Renewable and Sustainable Energy Reviews* 110, 378-391. DOI: 10.1016/j.rser.2019.05.003.

Sangaré, D., Belandria, V., Bostyn, S., Moscosa-Santillan, M., and Gökalp, I. (2024a). "Pyro-gasification of lignocellulosic biomass: Online quantification of gas evolution with temperature, effects of heating rate, and stoichiometric ratio," *Biomass Conversion and Biorefinery* 14(8), 9763-9775. DOI: 10.1007/s13399-022-03103-x

Sangaré, D., Bostyn, S., Santillán, M. M., García-Alamilla, P., Belandria, V., and Gökalp, I. (2022). "Comparative pyrolysis studies of lignocellulosic biomasses: Online gas quantification, kinetics triplets, and thermodynamic parameters of the process," *Bioresource Technology* 346, 126598. DOI: 10.1016/j.biortech.2021.126598

Sangaré, D., Moscosa-Santillan, M., Bostyn, S., Belandria, V., De la Cruz Martínez, A., Van and De Steene, L. (2024b). Multi-step kinetic mechanism coupled with CFD modeling of slow pyrolysis of biomass at different heating rates," *Chemical Engineering Journal* 479, 147791. DOI: 10.1016/j.cej.2023.147791

Shahbaz, M., Yusup, S., Inayat, A., Ammar, M., Patrick, D. O., Pratama, A., and Naqvi, S .R. (2017). "Syngas production from steam gasification of palm kernel shell with subsequent CO_2 capture using CaO sorbent: An aspen plus modeling," *Energy & Fuels* 31(11), 12350-12357. DOI: 10.1021/acs.energyfuels.7b02670

Stefanidis, S. D., Kalogiannis, K. G., Iliopoulou, E. F., Michailof, C. M., Pilavachi, P. A., and Lappas, A. A. (2014). "A study of lignocellulosic biomass pyrolysis via the pyrolysis of cellulose, hemicellulose and lignin," *Journal of Analytical and Applied Pyrolysis* 105, 143-150. DOI: 10.1016/j.jaap.2013.10.013

Torres, C., Urvina, L., and de Lasa, H. (2019). "A chemical equilibrium model for biomass gasification. Application to Costa Rican coffee pulp transformation unit," *Biomass and Bioenergy* 123, 89-103. DOI: 10.1016/j.biombioe.2019.01.025

Upreti, S. R. (2017). *Process Modeling and Simulation for Chemical Engineers: Theory and Practice*, John Wiley & Sons, Hoboken, NJ, USA.

Van Hoecke, L., Boeye, D., Gonzalez-Quiroga, A., Patience, G. S., and Perreault, P. (2023). "Experimental methods in chemical engineering: Computational fluid dynamics/finite volume method—CFD/FVM," *The Canadian Journal of Chemical Engineering* 101(2), 545-561. DOI: 10.1002/cjce.24571

Vyazovkin, S., Chrissafis, K., Di Lorenzo, M. L., Koga, N., Pijolat, M., Roduit, B., Sbirrazzuoli, N., and Suñol, J. J. (2014). "ICTAC Kinetics Committee recommendations for collecting experimental thermal analysis data for kinetic computations," *Thermochimica Acta* 590, 1-23. DOI: 10.1016/j.tca.2014.05.036.

Wang, L., Weller, C. L., Jones, D. D., and Hanna, M. A. (2008). "Contemporary issues in thermal gasification of biomass and its application to electricity and fuel production," *Biomass and Bioenergy* 32(7), 573-581. DOI: 10.1016/j.biombioe.2007.12.007

Wen, C. Y., and Chaung, T. (1979). "Entrainment coal gasification modeling," *Industrial & Engineering Chemistry Process Design and Development* 18(4), 684-695. DOI: 10.1021/i260072a020.

Xie, J., Zhong, W., Jin, B., Shao, Y., and Liu, H. (2012). "Simulation on gasification of forestry residues in fluidized beds by Eulerian–Lagrangian approach," *Bioresource Technology* 121, 36-46. DOI: 10.1016/j.biortech.2012.06.080

Yan, B.-H., Cao, C.-X., Cheng, Y., Jin, Y., and Cheng, Y. (2014). "Experimental investigation on coal devolatilization at high temperatures with different heating rates," *Fuel* 117, 1215-1222. DOI: 10.1016/j.fuel.2013.08.016

Yang, M., Zhang, J., Zhong, S., Li, T., Løvås, T., Fatehi, H., and Bai, X.-S. (2022). "CFD modeling of biomass combustion and gasification in fluidized bed reactors using a distribution kernel method," *Combustion and Flame* 236, article 111744. DOI: 10.1016/j.combustflame.2021.111744

Zeng, X., Ueki, Y., Yoshiie, R., Naruse, I., Wang, F., Han, Z., and Xu, G. (2020). "Recent progress in tar removal by char and the applications: A comprehensive analysis," *Carbon Resources Conversion* 3, 1-18. DOI: 10.1016/j.crcon.2019.12.001

Zhang, Y., Zhao, Y., Gao, X., Li, B., and Huang, J. (2015). "Energy and exergy analyses of syngas produced from rice husk gasification in an entrained flow reactor," *Journal of Cleaner Production* 95, 273-280. DOI: 10.1016/j.jclepro.2015.02.053

Zhang, Y., Zhao, Y., Li, B., Gao, X., and Jiang, B. (2017). "Energy and exergy characteristics of syngas produced from air gasification of walnut sawdust in an entrained flow reactor," *International Journal of Exergy* 23(3), 244-262. DOI: 10.1504/ijex.2017.085772

Zhu, L., Zhang, Y., Lei, H., Zhang, X., Wang, L., Bu, Q., and Wei, Y. (2018). "Production of hydrocarbons from biomass-derived biochar assisted microwave catalytic pyrolysis," *Sustainable Energy & Fuels* 2(8), 1781-1790. DOI: 10.1039/c8se00096d

Article submitted January 4, 2025; Peer review completed: February 1, 2025; Revised version received: February 7, 2025; Accepted: February 9, 2025; Published: February 21, 2025.
DOI: 10.15376/biores.20.2.2844-2870